

Constantly renewing glacial lakes in the Kyrgyz Range, northern Tien Shan

Mirlan Daiyrov¹ and Chiyuki Narama²

¹Graduate School of Science and Technology, Niigata University, Niigata city, 950-2181, Japan

²Program of Field Research in the Environmental Sciences, Niigata University, Niigata city, 950-2181, Japan

Correspondence: Mirlan Daiyrov (mirlan085@gmail.com)

Received: 22 August 2024 – Discussion started: 11 October 2024

Revised: 15 December 2025 – Accepted: 19 December 2025 – Published:

Abstract. In the Kyrgyz Range of the northern Tien Shan, Central Asia, glacial lakes have been a focus of monitoring due to the increasing concern over glacial lake outburst floods (GLOFs) in the context of notable glacier recession. This study investigates (1) the historical evolution in the number and area of glacial lakes larger than 0.00045 km² in 1968, 2000, and 2021 using Corona KH-4, Landsat 7/ETM+, and Sentinel-2 imagery, and (2) the relationship between lake development and the evolution of glacier-moraine complexes (GMCs) that contain buried ice. The number of glacial lakes doubled between 1968 and 2021, while their total area increased by 76 % from 0.80 to 1.42 km². Over the same period, 190 of the 274 lakes present in 1968 had disappeared by 2000. Many new lakes had formed by 2021, including one lake that reappeared after a prior disappearance since 1968 [TSI](#). Rapid lake formation was associated with a 31 % reduction in glacier area over the past 50 years and with GMC evolution. The expansion of GMCs and melting of buried ice within GMCs produced new surface depressions (thermokarst features), which subsequently filled with water to form lakes, resulting in continuous glacial lake renewal. Thus, the continuous renewal of glacial lakes in the Kyrgyz Range results from the combined effects of glacier retreat, GMC expansion, and buried-ice melt.

from satellite data (Kattel et al., 2020; Daiyrov et al., 2022). These lakes develop mainly on glacier-moraine complexes (GMCs; Shatravin, 2007; Erokhin, 2011), which formed during glacier retreat after the Little Ice Age (LIA). GMCs, also referred to as the ice-debris complexes (Bolch et al., 2018; Blöthe et al., 2021), are geomorphological units composed of buried ice and debris, and are characterized by the absence of distinct moraine ridges. Post-LIA climatic warming has induced geomorphological transformations in the recessional zones of glacier termini, where glacier ice has become isolated beneath debris as buried ice (Maksimov, 1982; Maksimov and Osmonov, 1995; Erokhin et al., 2017). As this buried ice has melted, numerous glacial lakes formed on GMCs, sometimes in direct contact with their parent glaciers, but often as independent thermokarst lakes (Janský et al., 2008). Lakes that are directly connected to glacier termini typically show faster expansion as a result of glacier recession, whereas lakes that do not have contact glaciers can also enlarge through the melting of dead ice within GMCs (Daiyrov et al., 2018; 2022). Approximately 20 % of these lakes are considered potentially hazardous (Janský et al., 2008, 2010).

Monitoring glacial lakes in the Kyrgyz Range is critical, because repeated GLOFs have caused severe damage (Erokhin, 2008, 2017; Kattel et al., 2020). Systematic research began in the 1960s, following catastrophic GLOF events in the Kyrgyz Republic. In the central part of the Kyrgyz Range, at least 22 GLOF events have been recorded since 1952 (Erokhin, 2011; Zaginaev et al., 2016), including recent floods and debris flows from Takyrtoz glacial lake on 5 June 2009, Teztor glacial lake on 31 July 2012, Chelektor glacial lake on 12 August 2017, Akpai glacial lake on 2

1 Introduction

The number of glacial lakes in high-mountain regions of Asia is rapidly increasing (Zhang et al., 2023). In the Kyrgyz Range, located in the northern Tien Shan of the Kyrgyz Republic, hundreds of glacial lakes have been identified

August 2021 (Erokhin et al., 2017; Kattel et al., 2020; Daiyrov et al., 2022), and Takyrtor glacial lake on 27 June 2025. These events have damaged infrastructure, agricultural fields, and downstream settlements (Erokhin et al., 2017; Zaginaev et al., 2019), highlighting the need for continuous hazard assessment (Kattel et al., 2020; Daiyrov et al., 2022). Compared to the eastern Himalayas, where the glacial lakes have been expanding continuously for decades (Yamada, 1998; Komori et al., 2004; Nagai et al., 2017), glacial lakes in the northern Tien Shan, including the Kyrgyz Range, are smaller and more susceptible to unstable, short-term fluctuations. This instability is influenced by geomorphological conditions such as drainage through ice tunnels within GMCs (Daiyrov et al., 2018; Narama et al., 2018). Despite their often small size, these lakes can pose significant hazards, especially because lakes described as “short-lived” (Narama et al., 2010, 2018; Daiyrov et al., 2018, 2022; Daiyrov and Narama, 2021) or “non-stationary” (Erokhin et al., 2017) may form and drain in rapid succession, sometimes occurring as catastrophic GLOFs.

The increase in glacial lakes has been reported across High Mountain Asia (HMA). However, the processes of glacial lake formation and the factors that trigger GLOFs vary considerably between regions. To accurately understand the relationship between glacial lake development and GLOFs, it is essential to clarify the distinctive characteristics of each locality. In the Kyrgyz Range, Central Asia, previous studies have documented the numbers and area of glacial lakes (Shatravin and Staviski, 1984; Janský et al., 2006; Usabaliev and Erokhin, 2007; Erokhin, 2008; Falatkova et al., 2019; Daiyrov et al., 2022). Despite these observations, long-term changes in glacial lakes and the processes that drive their renewal in this region remain insufficiently documented. To understand the characteristics of glacial lake formation history and to clarify the processes of rapid glacial lake renewal in the Kyrgyz Range, this study investigates (1) the historical evolution in the number and area of glacial lakes in 1968, 2000, and 2021 using Corona KH-4, Landsat 7/ETM+, and Sentinel-2 imagery, and (2) the relationship between lake development and the evolution of glacier-moraine complexes (GMCs) that contain buried ice. The latter relationship is investigated through analysis of glacier area changes derived from multi remote sensing datasets and digital elevation models (DEMs).

2 Study area

The study area is the Kyrgyz Range in the northern Tien Shan (Fig. 1), where mountain ridges range from 2500 to 4900 m above sea level. The central part, which contains many glaciers, is higher than the eastern and western parts. GMCs, formed after glacier retreat, are composed of buried ice and debris and are widely distributed at glacier fronts (Shatravin, 2007). These GMCs are distinct from debris-

covered glaciers. Lakes that form on GMCs are typically small, thermokarst-type, and non-stationary, although some are connected by internal drainage channels, and can trigger GLOFs (Narama et al., 2018). Some GMC termini have evolved into glacier-derived rock glaciers. Climate change over recent decades has caused shrinkage and degradation of both glaciers and GMCs (Erokhin et al., 2017; Daiyrov et al., 2018).

On the northern flank of the central part of the Kyrgyz Range, 483 glaciers covering approximately 520 km² between 3100 and 4200 m elevation have been identified, mainly in the Issyk-Ata, Alamudun, West-Karakol, and Sokuluk river basins (Maksimov and Osmonov, 1995; Usabaliev et al., 2013). In the Ala-Archa basin, glacier area decreased by 15.2%–18% between 1963/64 and 2003–2010 (Aizen et al., 2006; Bolch, 2015). Golubin Glacier (5.42 km²) is the largest in the Kyrgyz Range and has a long-term mass balance of -0.20 ± 0.42 m w.e. yr⁻¹ from 1949/50 to 2020/21 (Azisov et al., 2022). The largest GMC (~3 km²) is located at the Ken-Tor glacier front in the Noruz river basin (Figs. 1 and 6; Maksimov and Osmonov, 1995). Precipitation peaks between March and July, with an average annual precipitation of 787 mm and a mean annual temperature of -3.5 °C (1969–2005) at the Teo-Ashuu meteorological station (3400 m; Fig. 1) in the western part of the range. Precipitation is a critical factor controlling glacier mass balance in this region (Ponomarenko, 1976; Aizen et al., 2006).

3 Methods

3.1 Satellite data collection

To quantify historical changes in glacial lakes and glaciers in the Kyrgyz Range, we used a combination of satellite remote sensing datasets spanning five decades including Corona KH-4, Landsat 7/ETM+, and Sentinel-2 imagery. Thirteen near-cloud-free Corona KH-4 stereo photographs from 1964 and 1968 provide the earliest dataset, covering 2% (mainly 14 glaciers on the eastern part) and 98% of the study region, respectively. Each image covers about 16 km in width, with a spatial resolution between 1.8 and 2.7 m (Table 1). DEMs and orthoimages were generated from forward and aft stereo pairs using Metashape (Agisoft), and geometric distortions were corrected using a non-metric camera model. Ground control points (GCPs) for geometric correction were systematically selected on stable terrain features, such as large boulders, outside glacier and GMC areas. Coordinates were obtained from QuickBird imagery in Google Earth and from Advanced Land Observing Satellite/Panchromatic Remote Sensing Instrument for Stereo Mapping (ALOS/PRISM) orthoimages (2.5 m resolution) acquired in 2007, while vertical references were based on the High Mountain Asia (HMA) DEM (8 m resolution) from 2017. Each stereo pair, 25–30 GCPs were used, and grouped into four sub-areas (a–d), and

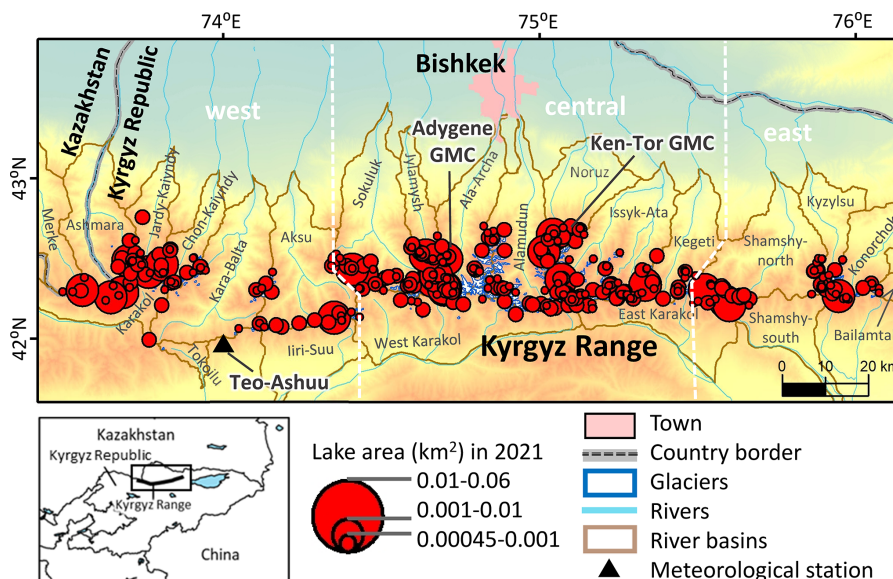


Figure 1. Maps of the study area in the Kyrgyz Range, northern Tien Shan. The upper map shows the Kyrgyz Range, with glacial lakes in 2021 indicated by red circles. The lower left map highlights the study sites in Kyrgyz Republic. The Kyrgyz Range is subdivided into three sections by white dotted lines, and the size of each glacial lake is represented by the diameter of its circle.

cloudy or snow-covered features were excluded to ensure accuracy. The final Corona-derived DEM and orthoimages have spatial resolutions of 4.1 and 2.0 m, respectively. We also used orthoimages from Landsat 7/ETM+ acquired in 2000 (15 m) and Sentinel-2 in 2021 (10 m; Table 2). Landsat 7/ETM+ pan-sharpened images were generated from 15 m panchromatic (band 8) and 30 m multispectral bands using ArcGIS Pro. Only scenes with minimal cloud or snow coverage were selected to maintain data quality and reliability.

3.2 Mapping of glacial lakes, glaciers, and GMCs

To assess changes in the area and number of glacial lakes in the Kyrgyz Range since 1960s, we manually digitized lakes from orthoimages of Corona KH-4 (1964, 1968), Landsat 7/ETM+ (2000), and Sentinel-2 (2021) imagery using ArcGIS Pro (Table 2). Manual mapping provides higher delineation accuracy than semi-automated methods, although boundary uncertainties remain at pixel-scale interfaces between water and land. Unclear lake outlines due to shadow in Corona imagery were evaluated using slope data from the Corona DEM to aid interpretation; areas with slopes $< 10^\circ$ within uncertain zones were included as lake area only when visually plausible, and otherwise excluded to avoid overestimation. Snow-covered and cloud-covered areas did not affect lake mapping because they did not coincide with lake locations.

We applied a series of preprocessing steps in ArcGIS Pro to ensure spatial and spectral consistency between Landsat 7/ETM+ and Sentinel-2 images. For stable land areas, we confirmed that pixel values from both sensors were compara-

ble and that normalized difference vegetation index (NDVI) values indicated similar vegetation cover, thereby ensuring that the datasets were suitable for temporal comparison. For image composition, Landsat 7/ETM+ bands 1, 2, and 3 were used to create an RGB composite for water detection, and lake outlines were mapped from Sentinel-2 imagery (10 m resolution) using the corresponding visible bands. To maintain consistency in lake detection across all dates, we adopted a minimum mapping threshold of 0.00045 km^2 , equivalent to two pixels of 15 m Landsat 7/ETM+ image, and applied this uniformly to Corona KH-4, Landsat 7/ETM+, and Sentinel-2 datasets. After manual delineation of lake boundaries, we calculated lake areas and classified each lake as either glacier-contact or contactless. Area changes for individual lakes were quantified for 1968, 2000, and 2021, and temporal shifts in lake type composition were also assessed.

Although manual mapping of lake polygons provides higher accuracy than semi-automated techniques, it remains sensitive to image-quality issues such as ambiguous margins at lake edges (Hanshaw and Bookhagen, 2014). This ambiguity occurs because pure-water pixels often border mixed pixels that contain both water and land, making edge classification difficult. To estimate area uncertainty, we followed Hanshaw and Bookhagen (2014) and excluded lakes with highly ambiguous boundaries from further analysis. To evaluate sensor-related uncertainty, we selected a stable reference lake outside the GMC zone that was clearly visible in all image types. Using consistent NDWI-based thresholds, we manually delineated this lake for each sensor and compared the mapped area. Landsat 7/ETM+ provided slightly larger lake areas than the 1968 Corona KH-4 reference (absolute dif-

Table 1. List of Corona KH-4 images in the study area.

Satellite	Corona Scenes	Date	Ground resolution (m)	Coverage area of study side and percentage
Corona KH-4A 10 (Corona 85, Mission 1010, OPS 3497)	DS1010-2086DA121 DS1010-2086DA120 DS1010-2086DF114 DS1010-2086DF115	20 September 1964	2.7	East part – 2 %
Corona KH-4A 48 (Corona 128, Mission 1048, OPS 0165)	DS1048-1039DA030 DS1048-1039DA031 DS1048-1039DA032 DS1048-1039DF030 DS1048-1039DF031 DS1048-1039DF032	18 September 1968	2.7–7.6	West, central and east part – 74 %
Corona KH-4B 4 (Corona 127, Mission 1104, OPS 5955)	DS1104-2185DF053 DS1104-2185DA057 DS1104-2185DA058	7 August 1968	1.8	Central-south part and east part – 24 %

Table 2. List of satellite images in the study area.

Satellite	Sensor	Date	Ground resolution (m)	ID:		
Landsat 7	Enhanced Thematic Mapper (ETM)	7 July 2000	30	LE07_L1TP_151031_20000707_20200918_02_T1		
		7 July 2000	30	LE07_L1TP_151030_20000707_20200918_02_T1		
		16 July 2000	30	LE07_L1TP_150030_20000716_20200918_02_T1		
		16 July 2000	30	LE07_L1TP_150031_20000716_20200918_02_T1		
		30 July 2000	30	LE07_L1TP_152031_20000730_20200917_02_T1		
		30 July 2000	30	LE07_L1TP_152030_20000730_20200918_02_T1		
		24 August 2000	30	LE07_L1TP_151031_20000824_20200918_02_T1		
		24 August 2000	30	LE07_L1TP_151030_20000824_20200917_02_T1		
		2 September 2000	30	LE07_L1TP_150031_20000902_20200917_02_T1		
		2 September 2000	30	LE07_L1TP_150030_20000902_20200918_02_T1		
		Sentinel-2	Multi-Spectral Instrument (MSI)	24 July 2021	10	S2A_MSIL2A_20210724T054641_N0500_R048_T43TEH_20230220T005731.SAFE
				11 August 2021	10	S2B_MSIL2A_20210811T055639_N0500_R091_T43TCH_20230215T033526.SAFE
11 August 2021	10			S2B_MSIL2A_20210811T055639_N0500_R091_T43TCG_20230215T033526.SAFE		
11 August 2021	10			S2B_MSIL2A_20210811T055639_N0500_R091_T43TDH_20230215T033526.SAFE		
11 August 2021	10			S2B_MSIL2A_20210811T055639_N0500_R091_T43TDG_20230215T033526.SAFE		
11 August 2021	10			S2B_MSIL2A_20210811T055639_N0500_R091_T43TEH_20230215T033526.SAFE		
21 August 2021	10			S2B_MSIL2A_20210821T055639_N0500_R091_T43TCH_20230210T193704.SAFE		
21 August 2021	10			S2B_MSIL2A_20210821T055639_N0500_R091_T43TCG_20230210T193704.SAFE		
21 August 2021	10			S2B_MSIL2A_20210821T055639_N0500_R091_T43TDH_20230210T193704.SAFE		
21 August 2021	10			S2B_MSIL2A_20210821T055639_N0500_R091_T43TDG_20230210T193704.SAFE		
21 August 2021	10			S2B_MSIL2A_20210821T055639_N0500_R091_T43TEH_20230210T193704.SAFE		
5 September 2021	10			S2A_MSIL2A_20210905T055641_N0500_R091_T43TCG_20230118T130151.SAFE		
5 September 2021	10			S2A_MSIL2A_20210905T055641_N0500_R091_T43TEH_20230118T130151.SAFE		
7 September 2021	10			S2B_MSIL2A_20210907T054639_N0500_R048_T43TEH_20230118T203059.SAFE		
27 September 2021	10			S2B_MSIL2A_20210927T054639_N0500_R048_T43TEH_20230124T140016.SAFE		

ference: 0.000326 km²; relative difference: 8.8 %), whereas Sentinel-2 (2021) provided results closer to the reference (absolute difference: 0.000127 km²; relative difference: 3.4 %). The finer spatial resolution of Sentinel-2 contributed to more precise boundary delineation. An uncertainty of about 8.8 % was considered acceptable for manual glacial lake mapping using Landsat 7/ETM+ data, and this reference lake was used to represent overall sensor-related error. The consistency of

these estimates with previous work in the Kyrgyz Range supports the robustness of our approach (Daiyrov et al., 2022).

Glaciers were also mapped manually using Corona KH-4 imagery from 1964 and 1968, and Sentinel-2 imagery from 2021. To ensure reliable boundary identification, we used only scenes with minimal cloud and snow cover. All Corona KH-4 imagery from 1968 and Sentinel-2 imagery from 2021 were acquired in summer (August for Sentinel-2, August–

September for Corona KH-4), thereby minimizing the influence of seasonal snow (Table 1). Glacier outlines were delineated by visual interpretation of standard false-colour composites from multispectral imagery, and glacier area changes between 1964/1968 and 2021 were calculated from these polygonal datasets.

GMCs in the study area were mapped based on several geomorphological criteria. GMCs were identified as continuous debris-covered surfaces, up to 3 km long, extending from the glacier fronts, lacking distinct moraine ridges, and showing a convex cross-sectional profile. The absence or discontinuity of surface drainage channels at glacier fronts was checked from Google Earth imagery. The presence of preserved ice within GMCs was further assessed using differential interferometric SAR (DInSAR) to detect surface deformation. These GMCs formed during glacier retreat after the Little Ice Age and typically consist of buried ice and debris (Shatravin, 2007; Erokhin, 2011). GMCs boundaries were delineated according to these geomorphological characteristics and previously published regional mapping (Maksimov, 1982; Maksimov and Osmonov, 1995; Shatravin and Staviski, 1984; Shatravin, 2007; Erokhin, 2008, 2011). GMCs were manually digitized mainly from Sentinel-2 imagery acquired in 2021, and higher-resolution Corona KH-4 images from 1964 and 1968 used where Sentinel-2 image quality was insufficient. All area delineations were performed on false-colour multispectral composites acquired under conditions of minimal cloud and snow cover.

3.3 Geomorphological analysis using DInSAR

To quantify GMCs that contain buried ice, we conducted DInSAR analysis using GAMMA SAR software and ALOS/Phase Array type L-band Synthetic Aperture Radar (PALSAR) and ALOS-2/PALSAR-2 (L-band) datasets. GMCs showing surface displacement in the form of coherent interference fringes, representing horizontal and vertical ground motion, were interpreted as likely containing significant ice content. These displacement fringes indicate active surface processes such as permafrost creep or subsidence caused by the melting of buried ice. In addition, landform features such as thermokarst depressions, curved ice cliffs, and surface channels were also considered in the mapping of GMCs. Data processing and interpretation followed established methods from previous studies (Goldstein and Werner, 1997; Werner et al., 2000; Quincey et al., 2007; Sandwell et al., 2008; Daiyrov et al., 2018).

We used both long-interval (> 10 months, spanning winter) and short-interval (1–3 months, summer) interferometric pairs, comprising 49 images in total (18 from ALOS/PALSAR images from 2009–2010 and 31 ALOS-2/PALSAR-2 images from 2014–2016), all with perpendicular baselines < 1500 m (Table 3). The DInSAR workflow included conversion of raw SAR data to Single Look Complex (SLC) format, coregistration of image pairs, generation of differ-

ential interferograms, removal of topographic phase using Shuttle Radar Topography Mission (SRTM) DEM, phase wrapping to obtain displacement, and geocoding to a geographic coordinate system. Noise from temporal and spatial decorrelation was reduced using an adaptive filter (Goldstein and Werner, 1997; Goldstein and Werner, 1998). In our results, long-interval interferograms mainly captured slow subsidence, whereas short-interval interferograms highlighted more rapid surface motion, consistent with earlier observations from rock glacier such as the Gruben rock glacier in the Swiss Alps, where only short-interval interferograms clearly detected surface motion (Strozzi et al., 2004).

DInSAR applications in high mountains is subject to limitations such as low scatterer density, atmospheric disturbances, and line-of-sight constraints, which can obscure displacement signals (Schlögl et al., 2022). Although L-band data have advantages over shorter wavelengths, issues such as low coherence, radar shadow, and foreshortening still affect the results in steep terrain (Atwood et al., 2010; Chen et al., 2024). To validate the interpretation of buried ice within GMCs, we compared DInSAR-derived surface motion at the Chelektor Glacier front with locations of known internal ice and found good spatial correspondence. Additional validation was provided by GNSS measurements at the Adygene Glacier GMC in Ala-Archa river basin (Fig. 1), which supported the presence of active, ice-related deformation. Independent evidence from DInSAR and field survey in the Teskey Range has also confirmed ice-rich GMCs in the northern Tien Shan (Daiyrov et al., 2018). Areas showing pronounced deformation were also analyzed using DEM differencing (HMA, 2017 and UAV, 2018), which indicated substantial surface changes within mapped buried ice zones. Consequently, deformation detected by DInSAR in GMCs is interpreted as evidence of ice-rich conditions, with melt-induced subsidence as the most plausible mechanism (Daiyrov et al., 2018).

3.4 Geomorphological analysis using DEMs and their accuracy assessment

Widespread formation of surface depression (thermokarst feature) on glaciers and GMCs is attributed to surface subsidence caused by melting buried ice (Erokhin et al., 2017; Narama et al., 2010, 2018; Daiyrov et al., 2018; Daiyrov and Narama, 2021). To investigate long-term morphological changes of GMCs, we compared DEMs derived from Corona KH-4 (1968) and HMA DEMs (2017). In addition, unmanned aerial vehicle (UAV) surveys were conducted for GMC at the Chelektor Glacier in the central part of the Kyrgyz Range in the summers of 2018 (15 July) and 2023 (28 July), generating complementary high-resolution data. The 2018 survey mapped the entire GMC, whereas the 2023 survey focused mainly on the glacier terminus because of unfavourable weather conditions. UAV data acquired with a Phantom4 RTK platform (DJI) were processed

Table 3. List of ALOS data (a part of data) for DInSAR analysis.

Pair	Master ID	Slave ID	Master Date	Slave Date	Span (d)	Bperp (m)	Orbit	Offnadir angle (°)
A	ALOS2015180840-140903	ALOS2058650840-150624	03 September 2014	24 June 2015	294	100.4	Ascending	36.2
B	ALPSRP239030840	ALPSRP245740840	20 July 2010	4 September 2010	46	337	Ascending	34.3
C	ALPSRP079740840	ALPSRP240780840	24 July 2007	1 August 2010	1104	1332.7	Ascending	34.3
D	ALOS2064120840-150731	ALOS2074470840-151009	31 July 2015	9 October 2015	70	90.9	Ascending	32.5
E	ALOS2018580840-140926	ALOS2072400840-150925	26 September 2014	25 September 2015	364	-14.2	Ascending	28.2
F	ALPSRP236550840	ALPSRP243260840	3 July 2010	18 August 2010	46	143.3	Ascending	34.3
J	ALOS2072400840-150925	ALOS2115870840-160715	25 September 2015	15 July 2016	294	128	Ascending	28.2

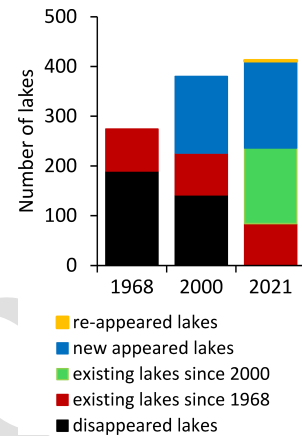
in Pix4Dmapper to generate orthoimages with a spatial resolution of 5.4 m and DEMs with a resolution of 1.0 m.

Vertical changes were quantified by comparing multiple DEMs: Corona KH-4 (4.1 m resolution, 1968), SRTM (30 m, 2000), HMA (8 m, 2017), and UAV DEMs (1.0 m, 2018 and 2023). Surface-depression polygons for 1968, 2000, 2017, 2018, and 2023 were generated using a hydrologic “filling” algorithm in ArcGIS Pro to allow quantitative assessment of depression area changes over time. The vertical accuracy of these datasets was evaluated relative to the HMA DEM, which was used as a stable reference. Stable, ice-free terrain outside GMCs was selected as benchmark areas, and elevations from Corona KH-4, SRTM, and UAV DEMs were vertically aligned to match HMA reference elevations, correcting systematic offsets. Elevation differences between each corrected DEM and the HMA DEM were then calculated within polygon area around the stable reference points. Root Mean Square Error (RMSE) values were 2.2 m for Corona DEM, 2.8 m for SRTM DEM, and 1.3 m for UAV DEM, which are acceptable for geomorphological analysis at the study scale and given the local relief. However, the relatively sparse GCPs for Corona KH-4 and the coarse resolution of SRTM limit the ultimate vertical precision of these datasets.

4 Results

4.1 Changes in glacial lake numbers and areas during 1968–2021

We identified 274 glacial lakes in 1968, 380 lakes in 2000, and 412 lakes by 2021 (Fig. 2), indicating that the number of lakes in the Kyrgyz Range nearly doubled over the study period. Of the 274 lakes present in 1968, 190 (69%) had disappeared by 2000, and of the 380 lakes mapped in 2000, 142 had disappeared by 2021. In contrast, 84 lakes persisted from 1968 through 2021. Substantial renewal occurred: 154 new lakes (41% of the total in 2000) appeared between 1968 and 2000, and a further 175 new lakes (42% of the total in 2021) formed between 2000 and 2021. Notably, one lake that had vanished by 2000 reappeared by 2021 (Fig. 2). The high rates of both lake disappearance and formation indicate a highly dynamic regime of glacial lake renewal, in contrast

**Figure 2.** Numbers of glacial lakes and their changes in 1968, 2000 and 2021.

to the more gradual and continual expansion of glacial lakes reported for the eastern Himalayas since the mid-twentieth century (Yamada, 1998; Ageta et al., 2000; Iwata et al., 2002; Komori et al., 2004). This pattern of rapid lake formation and loss is consistent with trends reported for the Kungoy and Ili Ranges, also within the northern Tien Shan (Narama et al., 2009).

Figure 3 shows the distribution of lakes by size class over time. In 1968, small lakes (0.00045–0.001 km²) accounted for 36% of all glacial lakes, but this proportion declined to 18% in 2000 and 22% in 2021. Medium-sized lakes (0.001–0.01 km²) dominated the total lake area, contributing 60% of the total lake area in 1968, 78% in 2000, and 71% in 2021. The number of large lakes (0.01–0.1 km²) increased from 11 in 1968 to 30 in 2021, and their total area of these lakes expanded 2.6-fold, from 0.23 km² to 0.59 km². In comparison, 773 glacial lakes larger than 0.1 km² have been identified in the Bhutan Himalayas (Nagai et al., 2017), whereas no glacial lakes exceeding 0.1 km² are present in the Kyrgyz Range.

The cumulative lake area increased from 0.80 km² in 1968 to 1.20 km² in 2000, and then by a further 18% to 1.42 km² by 2021. Among the 84 lakes that persisted for the entire study period, 14 showed marked variability, with area changes of 0.005–0.053 km² between 1968 and 2021. Of

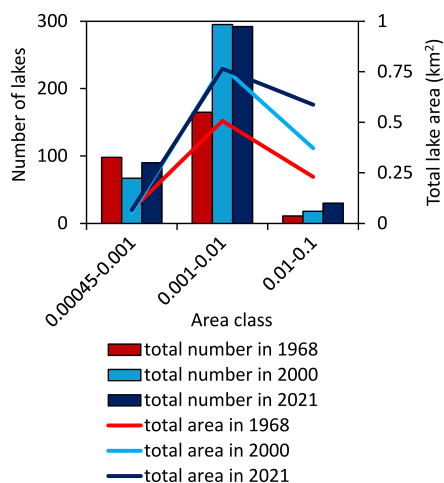


Figure 3. Numbers and areas of glacial lakes in the three area classes in 1968, 2000 and 2021.

the lakes present in 2000, 152 experienced changes in area, including 13 that showed pronounced increases of 0.005–0.053 km² between 2000 and 2021. Spatial analysis shows that the largest lakes formed predominantly at the termini of retreating glaciers, while most medium and small lakes developed on GMCs located farther from the current glacier termini.

4.2 Types of glacial lakes and their evolution

In this region, glacial lakes were classified into two main types based on their spatial relationship to glaciers: glacier-contact (proglacial) lakes and contactless (thermokarst) lakes (Fig. 4a). The classification was determined solely by the current position of each lake relative to the glacier margin, rather than by differences in origin. Glacier-contact lakes are located adjacent to glacier termini and are typically impounded by GMCs, moraines, or bedrock. In contrast, contactless lakes – primarily thermokarst in origin – form on the surface of GMCs as a result of the melting of buried ice. Some thermokarst lakes show pronounced seasonal variations in surface area, including phases of stability, expansion, shrinkage, appearance, disappearance, and short-lived existence (Daiyrov et al., 2018), similar to supraglacial lakes on debris-covered glaciers because of their connection to evolving drainage channels (Narama et al., 2017; Sakurai et al., 2021). More detailed classifications of lake types in the study area have been provided in previous reports (Erokhin, 2008, 2011; Janský et al., 2006, 2010).

Long-term analysis reveals a notable shift in lake types over time (Fig. 4b). Of the 274 lakes identified in 1968, 45 % (124 lakes) were contactless; this proportion increased to 72 % (272 of 380) in 2000 and 71 % (291 of 412) in 2021, indicating a significant increase in the number of thermokarst lakes on GMCs. Conversely, the number of glacier-contact lakes has steadily decreased since 1968. As illustrated in

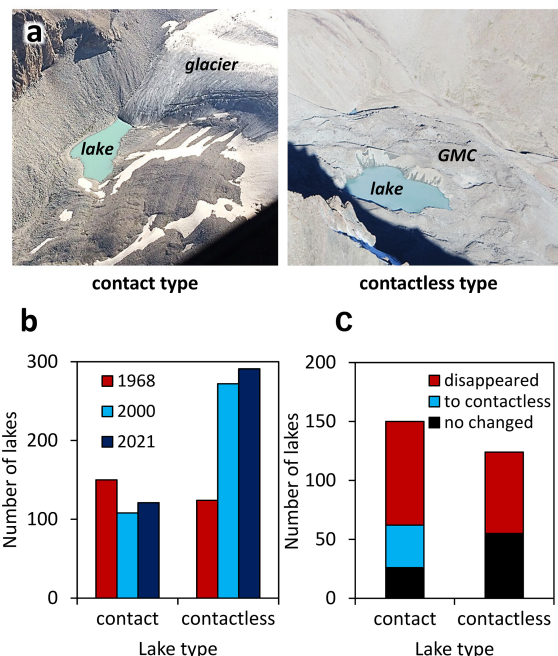


Figure 4. Number and transition of two types of glacial lakes. (a) Photographs of the two types of glacial lakes: glacier-contact (left) and contactless (right). (b) Comparison of the number of glacial lakes by type in 1968, 2000, and 2021. (c) Transitions in lake type from 1968 to 2021.

Fig. 4c, the evolution of individual lakes highlights these trends: of the 150 glacier-contact lakes present in 1968 (including one documented in 1964), only 26 remained glacier-contact by 2021, 36 had transitioned to contactless status due to glacier retreat, and 88 had disappeared. Of the 124 contactless lakes present in 1968, 55 persisted through 2021 while 69 disappeared.

These results indicate that, unlike the eastern Himalayas – where glacier-contact lakes can persist and expand over long periods (Yamada, 1998; Nagai et al., 2017) – glacier contact lakes in the Kyrgyz Range tend to be short-lived. Rapid glacier retreat combined with generally steep glacier-front slopes, often separates formerly contact lakes from glacier termini, while the limited development of large GMCs and flat outwash plains further restricts the sustained expansion and longevity of glacier-contact lakes (Agarwal et al., 2023).

4.3 Area changes in glaciers and surface changes in GMCs

To clarify the processes behind the recent formation and disappearance of glacial lakes, we analyzed temporal changes in both glacier extent and GMCs for the period 1968–2021. Substantial retreat of glacier termini occurred across the range, converting recently deglaciated area into GMCs (Fig. 5a). The total glacier area decreased from 378.5 km² in 1968 to 262.0 km² in 2021, reflecting a reduction of 31 %

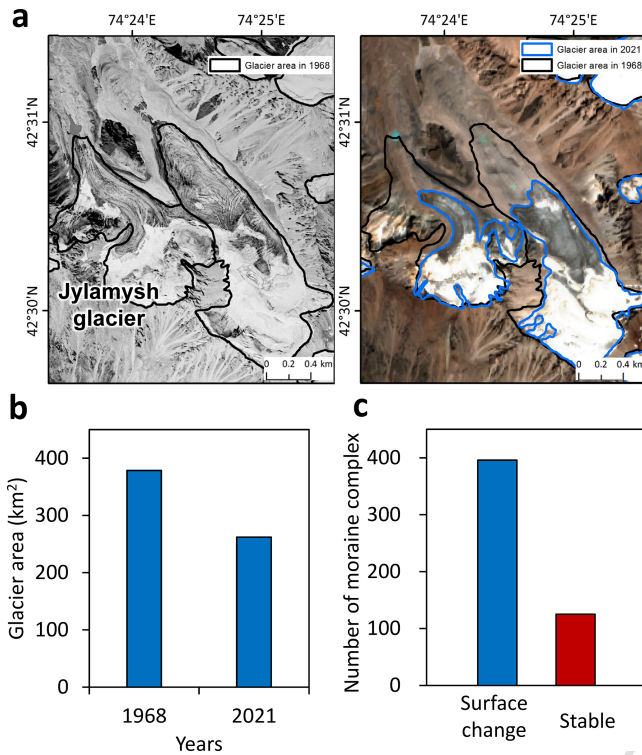


Figure 5. Glacier shrinkage and GMC conditions in the Kyrgyz Range. (a) Glacier shrinkage in the Kyrgyz Range, illustrated by satellite images from different years: Corona KH-4 (1968, left) and PlanetScope (2021, right). (b) Changes in glacier area in the Kyrgyz Range between 1968 and 2021. (c) Number of surface-detected GMCs based on DInSAR data. [TS2](#)

over 53 years (Fig. 5b). Spatially, 71 % of the glacierized area was concentrated in the central part of the Kyrgyz Range, while the western and eastern parts accounted for 19 % and 10 %, respectively. The relative shrinkage rates were 37 % in the central part, 27 % in the west, and 40 % in the east. Some large glaciers that retreat and separate into smaller glaciers within individual sub-catchments would normally increase the total glacier count (Bolch, 2015); however, the total number of glaciers decreased from 787 in 1968 to 757 in 2021. This net decrease reflects the disappearance of small glaciers after they separated from their parent glaciers. Glacier fragmentation often produced multiple GMCs within a single glacier basin, some of which evolved into independent units as the source glaciers completely disappeared (Shatravin, 2007; Erokhin, 2011). This process can also favored the formation of numerous small lakes (Izagirre et al., 2025). However, not all glaciers in the Kyrgyz Range have developed GMCs.

We identified 521 GMCs in the Kyrgyz Range. Focusing on GMCs that host numerous contactless (thermokarst) lakes, comparison of DEMs from Corona (1968) and HMA (2017) showed that 250 GMCs (41 % of the total) experienced substantial surface lowering of -5 to -30 m. Large

vertical declines (-10 to -30 m) were especially widespread in GMCs in the Sokuluk, Jylamysh, Ala-Archa, Alamudun, Noruz, Issyk-Ata, and Kegeti river basins (Fig. 1). DInSAR data for 2007–2010 and 2014–2016 further revealed that 396 (65 %) of 521 GMCs show significant displacement, consistent with deformation driven by melting buried ice (Fig. 5c; Daiyrov et al., 2018; Daiyrov and Narama, 2021). These DInSAR results also enabled identification of GMCs with high potential for future lake formation, as showing by displacement patterns on interferograms from summer 2009 and 2010 (Fig. 6). This significant surface changes occurred mainly on GMCs during summer and were closely related to subsidence from buried ice melt and creep of internal ice. The most pronounced deformation was observed in GMCs in the Sokuluk, Ala-Archa, and Issyk-Ata basins, whereas about 20 % of GMCs showed no detectable deformation, implying ice-free or only weakly active conditions. Areas without displacement were likely ice-free or degraded area (Buchelt et al., 2024; Kunz et al., 2022, 2025), indicating not all GMCs still contain buried ice.

At the Chelektor Glacier GMC, a representative site in the central part of the range, three surface depressions (thermokarst feature) formed between 1968 and 2017 (Fig. 7a, b). Morphological evidence from imagery and DEM differences clearly shows that ice melt induced both surface subsidence and depression formation (Fig. 7c). From 2000 to 2021, depression-1 expanded substantially (Fig. 7d), and repeat photographs from 2015 and 2018 capture the rapid morphological changes (Fig. 8a, b). Over this three-year interval, the surface area of the depression nearly doubled. Elevation profiles (Fig. 8c, f) reveal maximum surface lowering of -23 m for depression-1 and -28 m for depression-2, indicating substantial geomorphic modification. As the Chelektor Glacier retreated, new glacial lakes formed within these depressions, demonstrating the tight coupling between glacier retreat, GMC transformation, and lake formation (Fig. 8d, e).

4.4 Differences in glacial lake patterns among river basins

The evolution of lake numbers, glacier loss, and GMC area differs among the western, central, and eastern parts of the Kyrgyz Range (Fig. 9a). In the western and central parts, the number of glacial lakes increased steadily from 1968 to 2021, whereas a slight decrease in lake number was observed in the eastern part. The highest concentration of both glacial lakes and GMCs is distributed in the central part of the range, where glacier loss is also greatest.

Focusing on individual catchments in the central part of the Kyrgyz Range (Fig. 9b), most newly formed glacial lakes are concentrated in the Sokuluk, Ala-Archa, Alamudun and Issyk-Ata basins. Repeated formation of new surface depressions on GMCs, particularly in the Sokuluk, Jylamysh, Ala-Archa, Alamudun, and Issyk-Ata river basins, is associated with significant GMC surface changes and ongoing lake de-

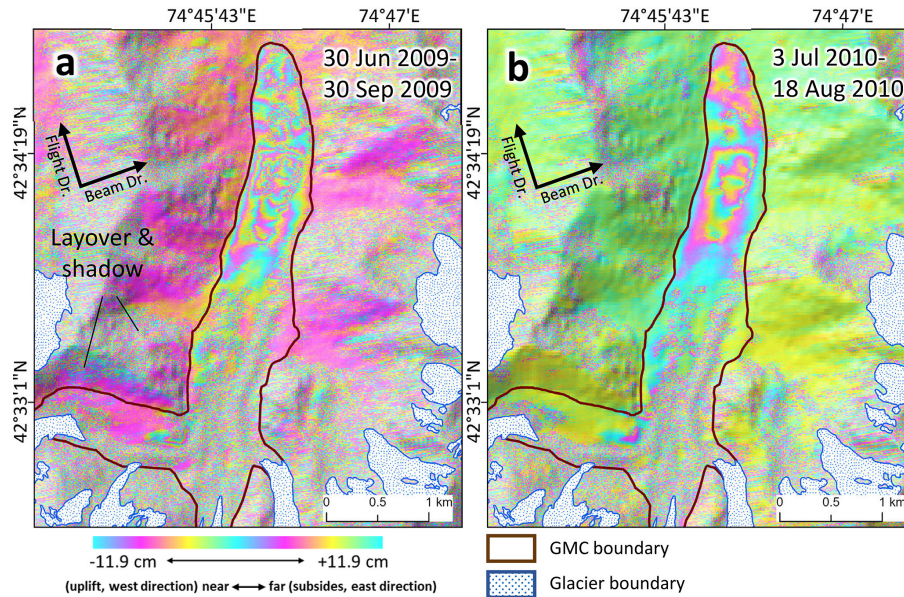


Figure 6. Surface change on the GMC based on DInSAR analysis in the summers of 2009 (a) and 2010 (b) using ALOS/PALSAR (Ken-Tor GMC, location in Fig. 1). The displacement patterns indicate subsidence and minor creep movements, which are interpreted as evidence of buried ice melt and surface instability.

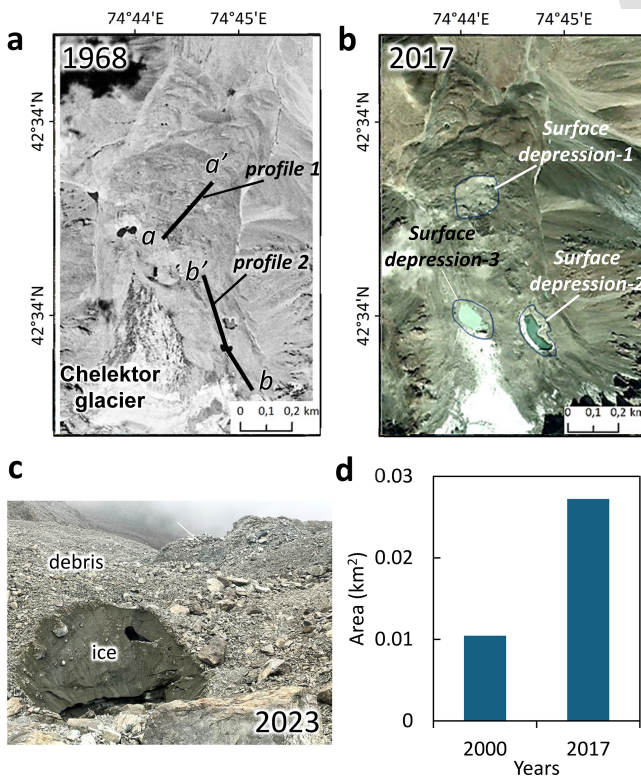


Figure 7. Development of surface depressions on the GMC at the Chelektor Glacier front (location in Fig. 1), illustrated by satellite images from different years: (a) Corona KH-4 (1968) and (b) PlanetScope (2017). (c) Exposed ice on the GMC. (d) Area changes of surface depression-1 from 2000 to 2017.

velopment. In contrast, the Shamschy-North basin in the east and Ak-Suu basin in the western part have more than 30 lakes, while all other catchments have fewer than 30. This concentration of active GMC evolution and thermokarst lake formation in the central part of the Kyrgyz Range indicates that this area is a key zone of rapid glacial lake renewal and elevated future GLOF hazard potential.

5 Discussion

5.1 Mechanisms underlying rapid glacial lake renewal

Between 2000 and 2021, 42 % of the glacial lakes in the Kyrgyz Range were newly formed (Fig. 2), indicating an exceptionally dynamic lake system. This rapid turnover is consistent with observation from the Kungoy and Ili Ranges in the northern Tien Shan (Narama et al., 2009). The primary driver is glacier shrinkage: glacier area has decreased by about 31 % over the past five decades, and newly deglaciated forcefields have developed into GMCs, greatly expanding potential area for lake formation (Fig. 5a).

The accelerated formation of contactless (thermokarst) lakes is further supported by the observed expansion and deepening of surface depressions (thermokarst features), resulting from the melting of buried ice within GMCs. At the Chelektor Glacier front, both downwasting and backwasting of buried ice have produced pronounced surface lowering and lateral enlargement of lake basins (Figs. 7, 8), similar to geomorphic processes observed on debris-covered glaciers elsewhere (Goldstein and Werner, 1997). Large depressions

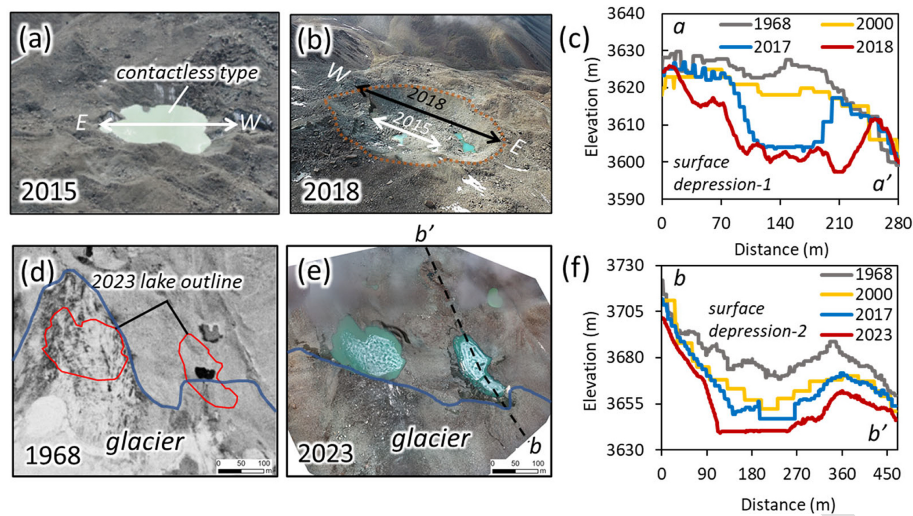


Figure 8. Surface depression development and the formation of new glacial lakes on GMC at the Chelektor glacier front. **(a, b)** Photographs of surface depression-1 in 2015 and 2018. **(c, f)** Changes in surface-depression profiles (profile lines indicated in Fig. 6a). **(d)** Orthoimage from Corona KH-4 (1968). **(e)** UAV orthoimage from 2023. Profile data are derived from DEMs of 1968 (Corona KH-4), 2000 (SRTM 1), 2017 (High Mountain Asia), and 2018–2023 (UAV data). [TS3](#)

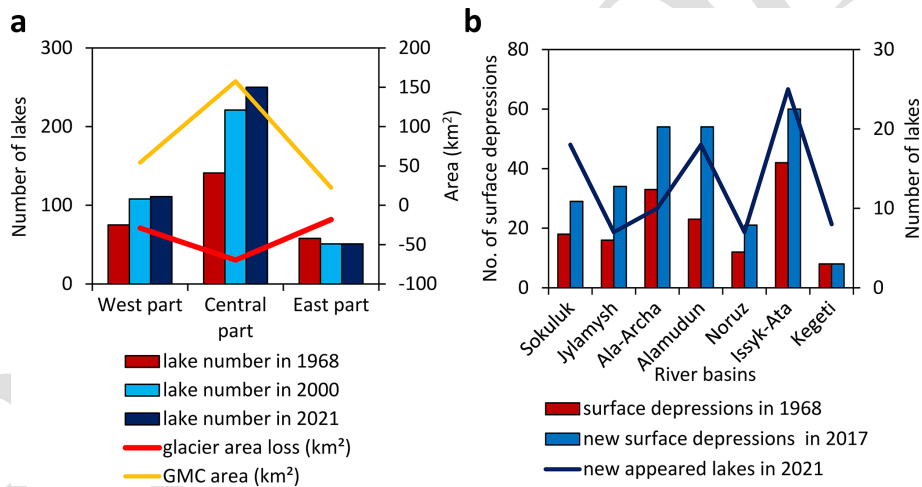


Figure 9. **(a)** Number of lakes in 1968, 2000, and 2021, and areas of glacier loss and GMCs in the three sections of the Kyrgyz Range. **(b)** Number of surface depressions in 1968 and 2017, and new lakes formed between 2000 and 2021 in the central part of the range.

formed as a result of glacier surface downwasting, as reported for the Teskey Range (Narama et al., 2010; Daiyrov et al., 2018), subsequently fill with meltwater and evolve into glacial lake.

In contrast to the eastern Himalayas, where glacier-contact lakes often persist and gradually expand for decades (Yamada, 1998; Ageta et al., 2000; Iwata et al., 2002; Komori et al., 2004; Nagai et al., 2017), glacier retreat in the Kyrgyz Range has mainly led to the disappearance of contact lakes or their transition to contactless types (Fig. 4c). As glacier retreat upslope, former contact lakes become isolated and lose direct meltwater supply, frequently resulting in their eventual disappearance. The persistence and reappearance of contact-

less lakes are controlled by local geomorphological conditions, including the existence of ice tunnels, buried ground ice, and the recurrent formation of surface depressions on GMCs. When meltwater or stream channels intersect these depressions, new thermokarst lakes can repeatedly form at the same location.

Recent climate warming has increased the sensitivity of GMCs to melting, accelerating depression formation and thereby promoting additional lake development (Daiyrov et al., 2018; Daiyrov and Narama, 2021). Consequently, GMCs must be regarded as key environments for future growth of contactless glacial lakes in the Kyrgyz Range (Falatkova et al., 2019). In the Himalayas, lake development is more di-

rectly associated with glacier shrinkage and the presence of large terminal moraines or broad outwash plains (Mool et al., 2001; Iwata et al., 2002; Yamada, 1998; Javed et al., 2025), and pro-glacial lakes connected to glaciers often show particularly rapid expansion (Ahmed et al., 2021). By contrast, the Kyrgyz Range, with its steep glacier forefields and ice-cored moraines, favors the rapid, recurrent formation of short-lived lakes—a tendency that is likely to intensify under continued warming and rising glacier equilibrium-line altitudes (Marchenko et al., 2007; Niederer et al., 2008). These characteristics underscore the strong control of glacier retreat and subsequent GMC evolution on the dynamics of glacial lake formation and persistence in the study region.

5.2 Regional variability in lake development

Glacial lake formation and turnover in the Kyrgyz Range are strongly concentrated in the central basins of Sokuluk, Ala-Archa, Alamudun, and Issyk-Ata, where dense and expanding GMCs coincide with rapid glacier shrinkage, leading to exceptionally high rates of lake appearance and disappearance and elevated hazard potential. This central part of the range has experienced most GLOF events over the past two decades (Erokhin et al., 2017; Kattel et al., 2020; Daiyrov et al., 2022), largely triggered by sudden drainage through ice tunnels within GMCs. These processes are characterized by frequent formation of surface depressions and subsequent thermokarst lake development, reflecting the influence of ice-rich GMC morphology and the ablation of buried ice. Detailed DInSAR and UAV survey data confirm that rapid surface lowering on GMCs in the central part of the range drives recurrent cycles of lake creation, whereas peripheral basins with fewer or more stable GMCs show much more limited changes in their lake systems.

Similar behaviour have been reported in nearby regions of the northern Tien Shan. In the Teskey Range, thermokarst lakes show rapid fluctuations in surface area that are closely associated with GMC conditions, with short-term lake variability linked to persistent ablation of buried ice and frequent transitions among lake types (Daiyrov et al., 2018; Daiyrov and Narama, 2021). Short-lived lakes have been responsible for most recent GLOFs in the Kyrgyz and Teskey Ranges, where triggers often involve temporary closure and reopening of ice tunnels within GMCs (Narama et al., 2010, 2018; Erokhin et al., 2017; Daiyrov et al., 2020, 2022). Tunnel blockage can result from debris deposition or freezing of water inside ice tunnels, with debris frequently supplied by melting dead ice in GMCs (Erokhin, 2011; Narama et al., 2018; Daiyrov and Narama, 2021). Thawing of buried ice through thermokarst processes leads to surface subsidence, collapse, and subsequent formation of distinctive thermokarst lakes (Kääb and Haeblerli, 2001). Thus, lake development in the Teskey Range – and likewise in the Kyrgyz Range – is fundamentally controlled by GMC conditions and the presence of large volumes of buried ice.

Given ongoing regional warming, further melting of dead ice within GMCs is expected, likely causing additional enlargement of depressions, accelerated lake formation, and an increased risk of sudden drainage events (GLOFs). Continuous monitoring and hazard assessment focused on GMC-rich catchments, particularly those with populated areas downstream, are thus essential, even though this study does not explicitly model future GLOF scenarios.

At the scale of High Mountain Asia (HMA), glacial lake expansion and related hazards are increasingly recognized. Furian et al. (2022) projected the formation of large proglacial lakes across HMA through 2100. Recent studies demonstrated accelerated glacial lake growth and have applied moraine-dam outburst models, particularly in the eastern Himalayas, for GLOF risk assessment (Zhang et al., 2023; Chen et al., 2024). However, the processes of lake formation and GLOF triggering in the Tien Shan differ fundamentally from those in the eastern Himalayas. Effective disaster-risk assessment and future projections therefore require (1) up-to-date, regional-specific records of lake development and GLOF history, and (2) a detailed understanding of the characteristic lake-formation processes specific to each mountain region.

6 Conclusions

This study quantifies the dynamic evolution of glacial lakes in the Kyrgyz Range, northern Tien Shan, over the period 1968–2021. During these 53 years, the number of glacial lakes increased from 274 in 1968 to 412 in 2021, nearly doubling, while total lake area expanded by 76%, from 0.80 to 1.42 km². Lake turnover was extremely high: of the 274 lakes present in 1968, 190 (69%) had disappeared by 2000. Despite these losses, 154 new lakes had appeared by 2000, and 175 more had formed by 2021, with only 84 lakes persisting throughout the entire study period. Over the same interval, glacier area shrank by 31% (from 378.5 to 262.0 km²), promoting widespread development of GMCs rich in buried ice. Surface lowering of about 5–30 m was observed in 41% of GMCs, and DInSAR analysis showed that 65% of GMCs exhibited measurable deformation, indicating active adjustment linked to buried-ice melt and favoring the rapid formation of new, often thermokarst, lakes. By 2021, over 70% of all glacial lakes were contactless types, reflecting the predominance of lake formation on GMCs rather than sustained proglacial lake expansion.

In the Kyrgyz Range, glacial lakes renew rapidly due to the combination of accelerated glacier retreat, the expansion of GMCs containing buried ice, and ongoing climate warming. As glaciers shrink, newly exposed GMCs with significant dead ice melt and subside, forming new surface depressions that are quickly filled with meltwater to create short-lived lakes. This geomorphological instability, coupled with repeated melting and reformation cycles, leads to a highly

dynamic regime in which glacial lakes frequently disappear, reappear, or form anew. The central part of the Kyrgyz Range, particularly the Sokuluk, Ala-Archa, and Issyk-Ata basins where many glaciers and GMCs are distributed, remains a hotspot for lake turnover and associated hazards. As warming continues, monitoring lake dynamics and GMC changes will be crucial for hazard assessment and adaptation in the region. Overall, the glacial lake system in the Kyrgyz Range is characterized by continual renewal driven by accelerated glacier retreat, GMC expansion and degradation, and ongoing climate warming, and that this regime stands in sharp contrast to the more gradual, persistent lake growth observed in regions such as the eastern Himalayas.

Code and data availability. Satellite image data such as Sentinel-2 and Landsat 7 are freely available from ESA (Copernicus Hub)^{TS4} and USGS^{TS5}. The GAMMA software used for the processing of the SAR images is available at <https://www.gamma-rs.ch/software>^{TS6} (Gamma Remote Sensing, 2024^{TS7}).

Author contributions. MD: Conceptualization, Data curation, Formal Analysis, Funding acquisition, Investigation, Resources, Validation, Writing—original draft, Writing—review and editing. CN: Conceptualization, Funding acquisition, Investigation, Project administration, Writing—review and editing.

Competing interests. The contact author has declared that neither of the authors has any competing interests.

Disclaimer. Publisher's note: Copernicus Publications remains neutral with regard to jurisdictional claims made in the text, published maps, institutional affiliations, or any other geographical representation in this paper. The authors bear the ultimate responsibility for providing appropriate place names. Views expressed in the text are those of the authors and do not necessarily reflect the views of the publisher.

Acknowledgements. We thank two reviewers for their valuable comments and suggestions. This study used ALOS satellite image data from ALOS Research Announcement (RA) in the framework of JAXA EORC.

Financial support. This research has been supported by Grant-in-Aid for JSPS Fellows (grant no. 22F22006) of JSPS KAKENHI Grant and Grant-in-Aid for Scientific Research (B) (grant nos. 19H01372 and 23K22023) of MEXT KAKENHI Grant.

Review statement. This paper was edited by Sven Fuchs and reviewed by Jan-Christoph Otto and one anonymous referee.

References

- Agarwal, V., Wyk de Vries, M. V., Haritashya, U. K., Garg, S., Kargel, J. S., Chen, Y., and Shugar, D. H.: Long-term analysis of glaciers and glacier lakes in the Central and Eastern Himalaya, *Sci. Total Environ.*, 898, 165598, <https://doi.org/10.1016/j.scitotenv.2023.165598>, 2023.
- Ageta, Y., Iwata, S., Yabuki, H., Naito, N., Sakai, A., Narama, C., and Karma.: Expansion of glacier lakes in recent decades in the Bhutan Himalayas, in: *IAHS Publ.*, Wallingford, UK, 165–175, ISBN 978-1-901502-31-2, 2000.
- Ahmed, R., Wani, G. F., Ahmad, S. T., Sahana, M., Singh, H., and Ahmed, P.: A review of glacial lake expansion and associated glacial lake outburst floods in the Himalayan region, *Earth Systems and Environment*, 5, 695–708, 2021.
- Aizen, V. B., Kuzmichenok, V. A., Surazakov, A. B., and Aizen, E. M.: Glacier changes in the central and northern Tien Shan during the last 140 years based on surface and remote-sensing data, *Ann. Glaciol.*, 43, 202–213, <https://doi.org/10.3189/172756406781812465>, 2006.
- Atwood, D. K., Meyer, F., and Arendt, A.: Using L-band SAR coherence to delineate glacier extent, *Can. J. Remote Sensing*, 36, S186–S195, 2010.
- Azisov, E., Hoelzle, M., Vorogushyn, S., Saks, T., Usabaliev, R., Esenaman uulu, M., and Barandun, M.: Reconstructed centennial mass balance change for Golubin Glacier, northern Tien Shan, *Atmosphere*, 13, 954, <https://doi.org/10.3390/atmos13060954>, 2022.
- Blöthe, J. H., Halla, C., Schwalbe, E., Bottegai, E., Liaudat, D. T., and Schrott, L.: Surface velocity fields of active rock glaciers and ice-debris complexes in the Central Andes of Argentina, *Earth Surf. Process. Landf.*, 46, 504–522, <https://doi.org/10.1002/esp.5042>, 2021.
- Bolch, T.: Glacier area and mass changes since 1964 in the Ala-Archa Valley, Kyrgyz Ala-Too, northern Tien-Shan, *Ice Snow*, 129, 28–39, <https://doi.org/10.15356/IS.2015.01.03>, 2015.
- Bolch, T., Rohrbach, N., Kutuzov, S., Robson, B. A., and Osmonov, A.: Occurrence, evolution and ice content of ice-debris complexes in the Ak-Shiirak, Central Tien Shan revealed by geophysical and remotely-sensed investigations, *Earth Surf. Process. Landf.*, 44, 129–143, <https://doi.org/10.1002/esp.4487>, 2018.
- Buchelt, S., Kunz, J., Wiegand, T., and Kneisel, C.: Dynamics and internal structure of a rock glacier: Inferring relationships from the combined use of differential synthetic aperture radar interferometry, electrical resistivity tomography and ground-penetrating radar. *Earth Surface Processes and Landforms*, 49, 4743–4758, <https://doi.org/10.1002/esp.5993>, 2024.
- Chen, M., Chen, Y., Fang, G., Zheng, G., Li, Z., and Li, Y.: Risk assessment of glacial lake outburst flood in the Central Asian Tianshan Mountains, *Clim. Atmos. Sci.*, 7, 209, <https://doi.org/10.1038/s41612-024-00755-6>, 2024.
- Daiyrov, M. and Narama, C.: Formation, evolution, and drainage of short-lived glacial lakes in permafrost environments of the northern Teskey Range, Central Asia, *Nat. Hazards Earth Syst. Sci.*, 21, 2245–2256, <https://doi.org/10.5194/nhess-21-2245-2021>, 2021.
- Daiyrov, M., Narama, C., Yamanokuchi, T., Tadono, T., Kääh, A., and Ukita, J.: Regional geomorphological conditions related to recent changes of glacial lakes in the

- Issyk-Kul basin, northern Tien Shan, *Geosciences*, 8, 99, <https://doi.org/10.3390/geosciences8030099>, 2018.
- Daiyrov, M., Narama, C., Kääh, A., and Tadono, T.: Formation and outburst of Toguz-Bulak glacial lake in the north part of Teskey Range, Tien Shan, Kyrgyzstan, *Geosciences*, 10, 468, <https://doi.org/10.3390/geosciences10110468>, 2020.
- Daiyrov, M., Kattel, D. B., Narama, C., and Wang, W.: Evaluating the variability of glacial lakes in the Kyrgyz and Teskey Ranges, Tien Shan, *Front. Earth Sci.*, 14, 112–119, 2022.
- Erokhin, S.: Data report of glacial lakes in 2000–2008, in: *Inventory of Glacial Lakes*, Ministry of Emergency Situations of the Kyrgyz Republic, Bishkek, 819 pp., ISBN 978-9967-23-948-4, 2008 (in Russian).
- Erokhin, S.: Types of moraine complexes and Tien-Shan glaciation, *Izvestiya NAS KR*, Bishkek, 115–118, [TSS](https://doi.org/10.26907/2541-7746.2011.115-118), 2011 (in Russian).
- Erokhin, S., Zaginaev, V., Meleshko, A., Ruiz-Villanueva, V., Petrakov, D. A., and Chernomorets, S. S.: Debris flows triggered from nonstationary glacier lake outbursts: The case of the Teztor Lake complex (Northern Tien Shan, Kyrgyzstan), *Landslides*, 15, 83–98, <https://doi.org/10.1007/s10346-017-0862-3>, 2017.
- Falatkova, K., Šobr, M., Neureiter, A., Schöner, W., Janský, B., Häusler, H., Engel, Z., and Beneš, V.: Development of proglacial lakes and evaluation of related outburst susceptibility at the Adygine ice-debris complex, northern Tien Shan, *Earth Surf. Dynam.*, 7, 301–320, <https://doi.org/10.5194/esurf-7-301-2019>, 2019.
- Furian, W., Maussion, F., and Schneider, C.: Projected 21st-century glacial lake evolution in high mountain Asia, *Front. Earth Sci.*, 10, 821798, <https://doi.org/10.3389/feart.2022.821798>, 2022.
- Goldstein, R. M. and Werner, C. L.: Radar ice motion interferometry, in: *Proc. 3rd ERS ESA Symp.*, ESA SP-414, Florence, Italy, 969–972, ISBN 978-9290922889, 1997.
- Goldstein, R. M. and Werner, C. L.: Radar interferogram phase filtering for geophysical applications, *Geophys. Res. Lett.*, 25, 4035–4038, 1998.
- Hanshaw, M. N. and Bookhagen, B.: Glacial areas, lake areas, and snow lines from 1975 to 2012: status of the Cordillera Vilcanota, including the Quelccaya Ice Cap, northern central Andes, Peru, *The Cryosphere*, 8, 359–376, <https://doi.org/10.5194/tc-8-359-2014>, 2014.
- Iwata, S., Ageta, Y., Sakai, A., Narama, C., and Karma.: Glacial lakes and their outburst flood assessment in the Bhutan Himalaya, *Glob. Environ. Res.*, 6, 3–17, 2002.
- Izagirre, E., Casassa, G., Dussaillant, I., Miles, E. S., Wilson, R., Rada, C., Faria, S. H., and Antiguiedad, I.: Evolution of glacial lakes and southernmost GLOFs in the Cordillera Darwin and Cloue Icefields (Tierra del Fuego) between 1945–2024, *Front. Earth Sci.*, 13, 1641167, <https://doi.org/10.3389/feart.2025.1641167>, 2025.
- Janský, B., Šobr, M., and Erokhin, S. A.: Typology of high mountain lakes of Kyrgyzstan with regard to the risk of their rupture, *Limnol. Rev.*, 6, 135–140, 2006.
- Janský, B., Šobr, M., and Engel, Z., and Yerokhin, S.: High-altitude lake outburst: Tien-Shan case study, in: *Evolution of geographical systems and risk processes in the global context*, edited by: Dostál, P., Charles Univ. Prague, Faculty of Science, P3K Publishers, Prague, 113–127, ISBN 978-80-903587-8-2, 2008.
- Janský, B., Šobr, M., and Engel, Z.: Outburst flood hazard: Case studies from the Tien-Shan Mountains, Kyrgyzstan, *Limnol. Ecol. Manage. Inland Waters*, 40, 358–364, 2010.
- Javed, M., Böhner, J., and Hasson, S.: Mapping Glacial Lakes in the Western Himalayas Using an Enhanced Breakpoint Method and CubeSat Imagery, *PFG – Journal of Photogrammetry, Remote Sens. and Geoinf. Science*, 93, 401–419, 2025.
- Kääh, A. and Haerberli, W.: Evolution of a high-mountain thermokarst lake in the Swiss Alps, *Arct. Antarct. Alp. Res.*, 33, 385–390, <https://doi.org/10.1080/15230430.2001.12003445>, 2001.
- Kattel, D. B., Mohanty, A., Daiyrov, M., Wang, W., Mishra, M., Kulenbekov, Z., and Dawadi, B.: Evaluation of glacial lakes and catastrophic floods on the northern slopes of the Kyrgyz Range, *Mountain Research and Development*, 40, 3, <https://doi.org/10.1659/MRD-JOURNAL-D-19-00068.1>, 2020.
- Komori, J., Gurung, D. R., Iwata, S., and Yabuki, H.: Variation and lake expansion of Chubda Glacier, Bhutan Himalayas, during the last 35 years, *Bull. Glaciol. Res.*, 21, 49–55, <https://doi.org/10.5331/bgr.21.49> [TS9](https://doi.org/10.5331/bgr.21.49), 2004.
- Kunz, J., Ullmann, T., and Kneisel, C.: Internal structure and recent dynamics of a moraine complex in an alpine glacier forefield revealed by geophysical surveying and Sentinel-1 InSAR time series, *Geomorphology*, 398, 108052, <https://doi.org/10.1016/j.geomorph.2021.108052>, 2022.
- Kunz, J., Buchelt, S., Wiegand, T., Ullmann, T., and Kneisel, C.: Thrust moraines and rock glaciers: Relationships between subsurface structures and morphodynamics in Swiss glacier forefields dominated by glacier-permafrost interactions, *EGU sphere [preprint]*, <https://doi.org/10.5194/egusphere-2025-1671>, 2025.
- Maksimov, E. V.: Climate Change and Mountain Glaciation in the New Era, *Proc. Russian Geogr. Soc.*, 114, 2, [TS10](https://doi.org/10.26907/2541-7746.1982.114.2), 1982.
- Maksimov, E. V. and Osmonov, A. O.: Features of modern glaciation and glacier dynamics of the Kyrgyz Ala-Too, *Natl. Acad. Sci. Kyrgyz Rep., Tian Shan Phys.-Geogr. Stn. Inst. Geol., Bishkek, Ilim*, 200 pp., ISBN 5-8355-0845-X, 1995.
- Marchenko, S. S., Gorbunov, A. P., and Romanovsky, V. E.: Permafrost warming in the Tien Shan Mountains, Central Asia, *Glob. Planet. Change*, 56, 311–327, <https://doi.org/10.1016/j.gloplacha.2006.07.023>, 2007.
- Mool, P. K., Bajracharya, S. R., and Joshi, S. P.: Inventory of Glaciers, Glacial Lakes and Glacial Lake Outburst Floods, Monitoring and Early Warning Systems in the Hindu Kush-Himalayan Region: Nepal, ICIMOD & UNEP RRC-AP, ISBN 978-92-9115-331-2, <https://doi.org/10.53055/ICIMOD.1018>, 2001.
- Nagai, H., Ukita, J., Narama, C., Fujita, K., Sakai, A., and Tadono, T.: Evaluating the scale and potential of GLOF in the Bhutan Himalayas using a satellite-based integral glacier-glacial lake inventory, *Geosciences*, 7, 77, <https://doi.org/10.3390/geosciences7030077>, 2017.
- Narama, C., Severskiy, I., and Yegorov, A.: Current state of glacier changes, glacial lakes, and outburst floods in the Ile Ala-Tau and Kungöy Ala-Too ranges, northern Tien Shan Mountains, *Ann. Hokkaido Geogr.*, 84, 22–32, <https://doi.org/10.7886/hgs.84.22>, 2009.
- Narama, C., Duishonakunov, M., Kääh, A., Daiyrov, M., and Abdakhmatov, K.: The 24 July 2008 outburst flood at the western Zyndan glacier lake and recent regional changes in glacier lakes of the Teskey Ala-Too range, Tien Shan, Kyrgyzstan, *Nat. Haz-*

- ards Earth Syst. Sci., 10, 647–659, <https://doi.org/10.5194/nhess-10-647-2010>, 2010.
- Narama, C., Daiyrov, M., Tadono, T., Yamamoto, M., Kääh, A., Morita, R., and Ukita, J.: Seasonal drainage of supraglacial lakes on debris-covered glaciers in the Tien Shan Mountains, Central Asia, *Geomorphology*, 286, 133–142, 2017.
- Narama, C., Daiyrov, M., Duishonakunov, M., Tadono, T., Sato, H., Kääh, A., Ukita, J., and Abdrakhmatov, K.: Large drainages from short-lived glacial lakes in the Teskey Range, Tien Shan Mountains, Central Asia, *Nat. Hazards Earth Syst. Sci.*, 18, 983–995, <https://doi.org/10.5194/nhess-18-983-2018>, 2018.
- Niederer, P., Bilenko, V., Ershova, N., Hurni, H., Yerokhin, S., and Maselli, D.: Tracing glacier wastage in the Northern Tien Shan (Kyrgyzstan/Central Asia) over the last 40 years, *Climatic Change*, 86, 227–234, <https://doi.org/10.1007/s10584-007-9288-6>, 2008.
- Ponomarenko, P. N.: Atmospheric precipitation of Kyrgyzstan, *Hydrometeo Publ. House, Leningrad*, 134 pp., 1976.
- Quincey, D. J., Richardson, S. D., Luckman, A., Lucas, R. M., Reynolds, J. M., Hambrey, M. J., and Glasser, N. F.: Early recognition of glacial lake hazards in the Himalaya using remote sensing datasets, *Glob. Planet. Change*, 56, 137–152, 2007.
- Sakurai, N., Narama, C., Daiyrov, M., Esenamanov, M., Usekov, Z., and Inoue, H.: Simultaneous drainage events from supraglacial lakes on the southern Inylchek Glacier, Central Asia, *Journal of Glaciology*, 68, 209–220, <https://doi.org/10.1017/jog.2021.77>, 2021.
- Sandwell, D. T., Myer, D., Mellors, R., Shimada, M., Brooks, B., and Foster, J.: Accuracy and resolution of ALOS interferometry: Vector deformation maps of the Father's Day intrusion at Kilauea, *IEEE Trans. Geosci. Remote Sens.*, 46, 3524–3534, <https://doi.org/10.1109/TGRS.2008.2000634>, 2008.
- Schlögl, M., Gutjahr, K., and Fuchs, S.: The challenge to use multi-temporal InSAR for landslide early warning, *Nat. Hazards*, 112, 2913–2919, <https://doi.org/10.1007/s11069-022-05289-9>, 2022.
- Shatravin, V. I.: Reconstruction of Pleistocene and Holocene glaciations in the Tien-Shan from new starting positions, in: *Climate, Glaciers and Lakes: Journey to the Past*, Ilim, Bishkek, 26–46, 2007.
- Shatravin, V. I. and Staviski, J. S.: Methodological bases for the identification of settling factors during detailed studies of high-altitude lakes, *Selevye Potoki, Hydrometeorolog. Publ. House*, 83–92, ISBN 978-5-286, 1984.
- Strozzi, T., Kääh, A., and Frauenfelder, R.: Detecting and quantifying mountain permafrost creep from in situ inventory, space-borne radar interferometry and airborne digital photogrammetry, *Int. J. Remote Sens.*, 25, 2919–2931, <https://doi.org/10.1080/0143116042000192330>, 2004.
- Usabaliev, R. and Erokhin, S.: Formation of high-mountainous lakes as a consequence of the degradation of the modern glaciation of the Tien Shan, in: *Materials of glaciological studies*, 103, 134–137, 2007.
- Usabaliev, R., Chen, X., and Osmonov, A.: The geography of glaciation of the mountains of Kyrgyzstan, in: *Physical geography of Kyrgyzstan*, Bishkek, Turar Publ. House, 133–210, ISBN 978-5-4470-0132-2, 2013.
- Werner, C., Wegmüller, U., Strozzi, T., and Wiesmann, A.: Gamma SAR and interferometric processing software, in: *ERS-ENVISAT Symp.*, Gothenburg, Sweden, edited by: Sawaya-Lacoste, H., ESA Publ. Div., Noordwijk, ISBN 92-9092-690-2, 2000.
- Yamada, T.: Glacier lake and its outburst flood in the Nepal Himalaya, Data Center for Glacier Research, Japanese Society of Snow and Ice, Monograph No. 1, Tokyo, **TS11**, 1998.
- Zaginaev, V., Ballesteros-Cánovas, J., Matov, E., Petrakov, D., and Stoffel, M.: Reconstruction of glacial lake outburst floods in northern Tien-Shan: Implications for hazard assessment, *Geomorphology*, 269, 75–84, <https://doi.org/10.1016/j.geomorph.2016.06.028>, 2016.
- Zaginaev, V., Falatkova, K., Jansky, B., Sobr, M., and Erokhin, S.: Development of a potentially hazardous pro-glacial lake in Ak-say valley, Kyrgyz Range, northern Tien Shan, *Hydrology*, 6, 3, <https://doi.org/10.3390/hydrology6010003>, 2019.
- Zhang, T., Wang, W., An, B., and Wei, L.: Enhanced glacial lake activity threatens numerous communities and infrastructure in the Third Pole, *Nat. Commun.*, 14, 8250, <https://doi.org/10.1038/s41467-023-44123-z>, 2023.

Remarks from the typesetter

- TS1** Due to the requested changes, we have to forward your requests to the handling editor for approval. To explain the corrections needed to the editor, please send me the reason why these corrections are necessary. Please note that the status of your paper will be changed to "Post-review adjustments" until the editor has made their decision. We will keep you informed via email.
- TS2** Due to the requested changes, we have to forward your requests to the handling editor for approval. To explain the corrections needed to the editor, please send me the reason why these corrections are necessary. Please note that the status of your paper will be changed to "Post-review adjustments" until the editor has made their decision. We will keep you informed via email.
- TS3** Please clarify what needs to be changed in Fig. 8 as this might need editor approval. Please note that mere stylistic changes are not possible at this stage.
- TS4** Please indicate how this data set can be accessed/obtained.
- TS5** Please indicate how this data set can be accessed/obtained.
- TS6** Please provide date of last access.
- TS7** Please provide the missing reference list entry.
- TS8** Please note that an ISSN cannot be inserted as a persistent identifier for this publication. Please check if you can provide a direct link to the article (incl. the date of last access).
- TS9** An ISSN cannot be used here. Please check if you can provide the correct DOI.
- TS10** Please note that an ISSN cannot be inserted as a persistent identifier for this publication. Please check if you can provide a direct link to the article (incl. the date of last access).
- TS11** Please note that an ISSN cannot be inserted as a persistent identifier for this publication. Please check if you can provide a direct link (URL) to the article (incl. the date of last access).